AN ABSTRACT OF THE THESIS OF

Ethan W. Dereszynski for the degree of Masters of Science in Computer Science presented on October 25th, 2007.

Title: A Probabilistic Model for Anomaly Detection in Remote Sensor Streams

Abstract approved: ______________________________

Thomas G. Dietterich

Remote sensors are becoming the standard for observing and recording ecological data in the field. Such sensors can record data at fine temporal resolutions, and they can operate under extreme conditions prohibitive to human access. Unfortunately, sensor data streams exhibit many kinds of errors ranging from corrupt communications to partial or total sensor failures. This means that the raw data stream must be cleaned before it can be used by domain scientists. In our application environment—the H.J. Andrews Experimental Forest—this data cleaning is performed manually. This thesis introduces a Dynamic Bayesian Network model for analyzing sensor observations and distinguishing sensor failures from valid data for the case of air temperature measured at a 15-minute time resolution. The model combines an accurate distribution of seasonal, long-term trends and temporally localized, short-term temperature variations with a single generalized fault model. Experiments with historical data show that the precision and recall of the method is comparable to that of the domain expert.

A Probabilistic Model for Anomaly Detection in Remote Sensor Streams

by

Ethan W. Dereszynski

A THESIS

submitted to

Oregon State University

in partial fulfillment of
the requirements for the
degree of

Masters of Science

Presented October 25th, 2007
Commencement June 2008

Masters of Science thesis of Ethan W. Dereszynski presented on October 25th, 2007.

APPROVED:

Major Professor, representing Computer Science

Director of the School of Electrical Engineering and Computer Science

---

Dean of the Graduate School

I understand that my thesis will become part of the permanent collection of Oregon State University libraries. My signature below authorizes release of my thesis to any reader upon request.

Ethan W. Dereszynski, Author

ACKNOWLEDGEMENTS

The author would like to thank Frederick Bierlmaier and Donald Henshaw for providing us with the raw and processed atmospheric data from the H.J. Andrews LTER and for their help in discerning the anomaly types found therein. This work was supported under the NSF Ecosystem Informatics IGERT (grant number DGE-0333257).

TABLE OF CONTENTS

TABLE OF CONTENTS (Continued)

LIST OF FIGURES

LIST OF TABLES

DEDICATION

This work is dedicated to my father, Gerald James Dereszynski. His strength and guidance has brought me to this day, and I pray it will be with me for all the days to come.

Chapter 1 – Introduction

The ecosystem sciences are on the brink of a huge transformation in the quantity of sensor data that is being collected and made available via the web. Old sensor technologies that measure temperature, wind, precipitation, and stream flow at a small number of spatially distributed stations are being augmented by dense wireless sensor networks that can measure everything from sapflow to gas concentrations. Data streams from existing and new sensor networks are being published to public servers for dispersion to the scientific community. The resultant surge in data is likely to transform ecology from an analytical and computational science into a data exploration science [30].

Unfortunately, raw sensor data streams can contain many kinds of errors from a variety of potential sources. Sensors can be damaged by extreme weather, information can be corrupted during data transmission, and environmental conditions and technical errors can change the meaning of the sensor data (e.g., an air temperature sensor buried in snow is no longer measuring air temperature, two thermometers whose cables are swapped during maintenance will not be measuring the intended temperatures, etc.). In current practice, data streams undergo a quality assurance (QA) process before they are made available to scientists. This is typically a manual process in which an expert technician visualizes the data in various ways looking for outliers, unusual events, and so on. But this manual approach has two obvious drawbacks. First, it is slow, expensive, and tedious. This introduces a substantial delay (3-6 months) between the time the data is collected and the time the data is made publicly available. Second, it will not scale up to the large amounts of data that will be collected by dense sensor networks. Hence, there is a need for automated methods for "cleaning" the data streams to flag suspicious data points and either call them to the attention of the technician or automatically remove incorrect values and impute corrected values.

This thesis describes a Dynamic Bayesian Network (DBN, [6]) approach to automatic data cleaning for individual air temperature data streams. The DBN combines discrete and conditional linear-Gaussian random variables to model the air temperature at 15 minute intervals as a function of diurnal, seasonal, and local trend effects. Because the set of potential faults is unbounded, it is not practical to approach this as a diagnosis problem where each fault is modeled separately [11]. Instead, we employ a very general fault model and focus our efforts on making the DBN model of normal behavior highly accurate. The hope is that if the observed temperature is unlikely based on the temperature model, the fault model will become more likely. The DBN contains two hidden variables: the current state of the sensor and the current temperature trend (as a departure from the baseline temperature). The model is applied online as a filter to decide the state of the sensor at each 15 minute point. If the sensor is believed to be bad, the observed temperature is ignored by the DBN until the sensor returns to normal. As a side effect, the model predicts what the true temperature was during periods of time when the sensor is bad.

This thesis is organized as follows. We first discuss some previous efforts in anomaly detection. Second, we describe the nature of the temperature data, the sensor sites at the H.J. Andrews Experimental Forest, and the anomaly types encountered. Then, we describe the temperature prediction model, including training and inference in Conditinal Linear-Gaussian networks. Finally, we present the results of the model applied to temperature data from the Andrews.

Chapter 2 – Previous Work

A simple (though common) approach to anomaly detection is to provide a visual representation of the data and allow a domain expert to manually inspect, label, and remove anomalies. In Mourand & Bertrand-Krajewski [21], this method is improved upon through the application of a series of logical tests to pre-screen the data. These tests include range-checks to insure the observations fall within reasonable domain limits, similar checks for the signal's gradient, and direct comparisons to redundant sensors. The goal is to ultimately reduce the amount of work the domain expert has to do to clean the data, which is consistent with our approach.

Temporal methods evaluate a single observation in the context of a time segment (sliding window) of the data stream or previous observations corresponding to similar periods in cyclical time-series data. The work i Reis et al. [28] uses a predictor for daily hospital visits based on multiday filters (linear, uniform, exponential) that lend varying weight to days in the current sliding window. The motivation for such an approach is to reduce the effect of isolated noisy events creating false positives or negatives in the system, as might occur with a single-observation-based classifier. In a similar vein, Wang et al. [31] construct a periodic autoregresive model (PAR, [3]), which varies the weights of a standard autoregressive model according to a set of user-defined periods within the time series. A daily visitation count is predicted by the PAR model, and if it matches the observed value, then the PAR model is updated with the observation; otherwise, the value is flagged as anomalous, an alarm is raised, and the observation is replaced with a uniformly smoothed value over a window containing the last several observations.

Spatial methods are useful in cases where there exist additional sensors distributed over a geographic area. The intuition is that if an explict spatial model exists that can account for the discrepencies between observed values at different sites, then these sensors can, in effect, be considered redundant. An example of this approach can be found in the work by Daly et al. [5], where each distributed sensor is held out from the remaining set of sensors, and its recorded observation validated againt an interpolated value from the remaining set.

Belief Networks [25] have been employed for sensor validation and fault detection in domains such as robotic movement, chemical reactors, and power plant monitoring [24, 20, 12]. Typically, the uncertainty in these domains is limited to the sensor's functionality under normal and inoperative conditions. That is, the processes in these domains function within some specified boundaries with a behavior that can be modeled by a system of known equations [13, 1]. Ecological domains are challenging because accurate process models encompassing all relevant factors are typically unavailable [9]; as such, uncertainty must be incorporated into both the process and sensor models.

Perhaps most related to our own work, Hill et al. use a DBN model to analyze and diagnose anomalous wind velocity data [10]. The authors explore individual sensor models as well as a coupled-DBN model that attempts to model the joint distribution of two sensors. The nature of the anomaly types in the data appear to be either short-term or long-term malfunctions in which the windspeed drastically increases or decreases; consequently, a first-order Markov process is sufficient to determine sharp rates of increase or decrease in windspeed. The joint distribution is modeled as a multivariate Gaussian conditioned on the joint state of respective sensors (represented as a discrete set of state pairs). Our approach primarily differs in that the nature of our data, and the corresponding anomaly types, requires a more sophisticated proces model that incorporates a baseline and a deviation component to account for anomalies not relating to sudden, dramatic shifts in the data. That is, our model must be robust enough to account for the strong seasonal and diurnal trends in the data while still detecting anomalous values.

Chapter 3 – Application Domain

We focus our application on twelve air temperature sensors distributed over three meteorological stations at the H.J. Andrews Experimental Forest, a Long Term Ecological Research (LTER) site located in the central Cascade Region of Oregon. The three meteorological stations—Primary, Central, and Upper Lookout—are located at elevations of 430 meters, 1005 meters, and 1280 meters, respectively. Figure 3.1 depicts the layout of the Andrews LTER, including the Primary, Central, and Upper Lookout Met stations (1, 2, and 3, respectively).

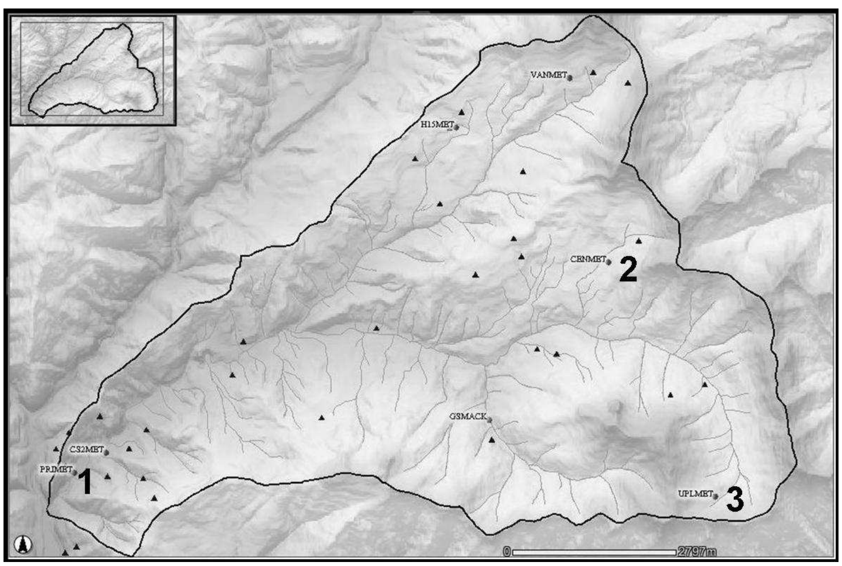

Figure 3.1: Andrews LTER and Meteorological Stations

Each site contains four air temperature sensors mounted on a sensor tower. The sensors are placed at heights of 1.5 meters, 2.5 meters, 3.5 meters, and 4.5

meters above ground level. The sensors record the ambient air temperature every 15 minutes and transmit the recorded value to a data logger located at the meteorological ("met") station. The logger periodically transmits the batch data back to a receiving station at the Andrews Headquarters, where it is reviewed by a domain expert before being made available for public download [19]. There are 96 observations (quarter-hour intervals) per day and 35,040 observations per year.

The observed air temperature data contains significant diurnal (time of day) and seasonal (day of year) effects. Temperature rises in the morning and falls in the evening (the diurnal effect). Temperatures are higher in the summer and colder in the winter (the seasonal effect). These effects interact so that in the summer, the diurnal effect is more pronounced—the temperature swings are larger and the temperature rises and falls faster—than in the winter. In addition, weather systems (cold fronts, heat waves) cause medium term (1-10 day) departures from the temperatures that would be expected based only on the diurnal and seasonal effects. Figure 3.2 illustrates diurnal, seasonal, and weather effects on air temperature. Week five and week thirty-two demonstrate the seasonal effect on air temperature (winter and summer, respectively), whereas week seven illustrates a weather event suppressing the diurnal effect for the first four days of the week.

3.1 Degrees of Anomaly

We classify anomaly types found in the air temperature data into three categories based on the degree of subtlety of the anomaly in the context of the data. Note

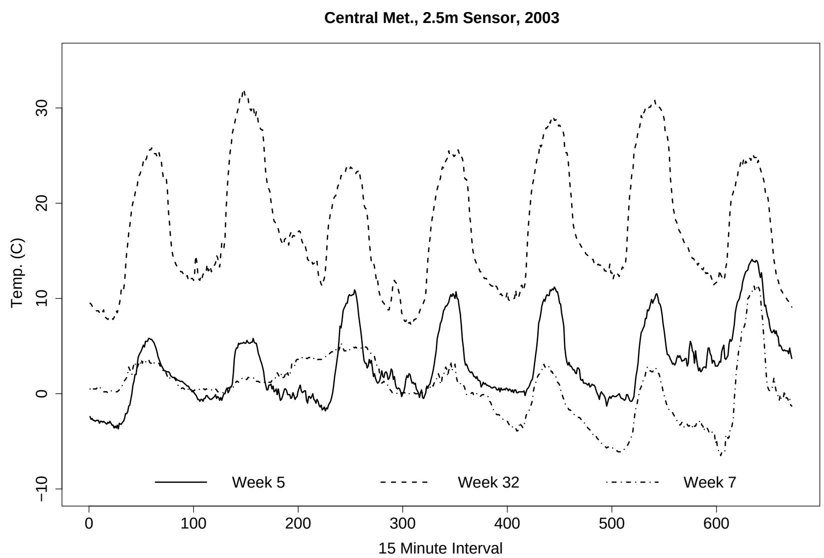

Figure 3.2: Seasonal, Diurnal, and Weather effects

that these classifications are purely for expository purposes to convey the difficulty of detection; we make no attempt to explicitly model these types in our system.

3.1.1 Simple Anomalies

We consider simple anomalies to be observations far outside the range of acceptable temperatures. These anomalies are introduced deliberately by the data logger. If the sensor is disconnected from the data logger, the logger records a value of −53.3 ℃. If the logger receives a voltage outside the measurement range for the sensor, the logger records a value of −6999 ℃. These two are the most common anomaly types, because sensor disconnections and damage to the wiring may persist for long periods of time depending on the accessibility of the sensor. For example, during the winter and during strong storms and floods, the Central and Upper Lookout stations are usually inaccessible. Figure 3.3 depicts two such anomalous periods.

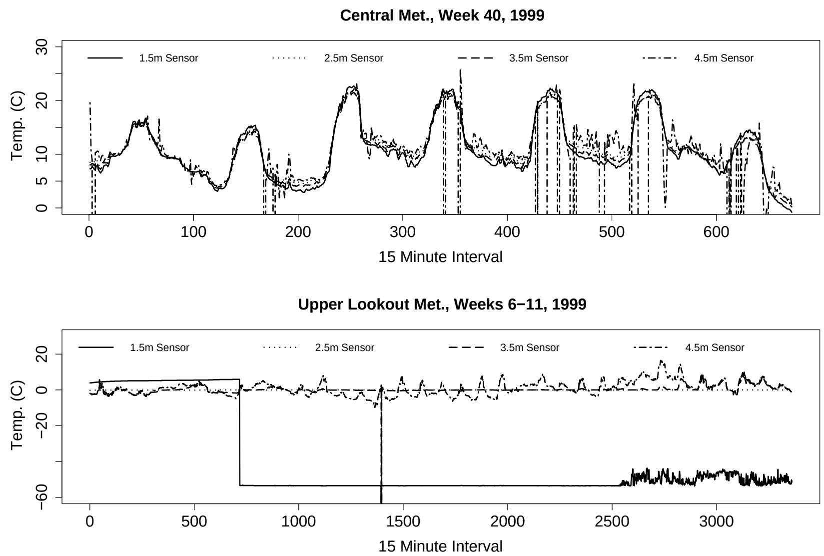

Figure 3.3: Top: 4.5m voltage out of range, −6999.9 ℃ fault value. Bottom: 1.5m disconnected from logger, −53.3 ℃ fault value

3.1.2 Medium Anomalies

This anomaly type is associated with malfunctions in the sensor hardware or change in functionality of the sensor. For example, if the sensor's sun shield becomes damaged or lost, then direct sunlight exposure introduces a positive bias in the recorded value. These anomaly types are correlated with external weather conditions and hence contain many of the same trend effects as the valid data, which makes them harder to detect. Figure 3.4 contains two such examples.

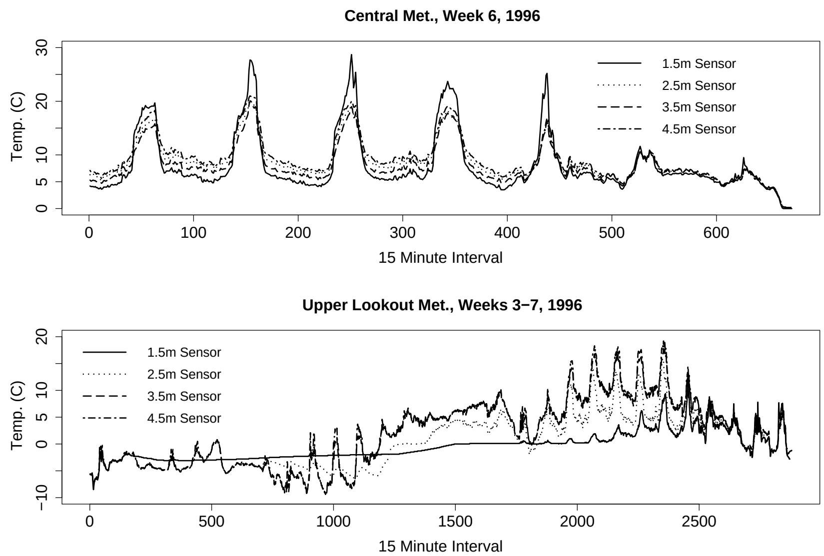

Figure 3.4: Top: Broken Sun Shield, Bottom: 1.5m Sensor buried under snowpack, 2.5m Sensor dampened

The first plot illustrates the loss of a sun shield on the 1.5m sensor, which raises the recorded temperature by approximately 5 ℃. It is important to note that this bias disappears during the night time periods and also on cloudy days (which probably explains why the bias is missing during the last two days of the week).

The second plot results from a snowpack that has buried the 1.5m sensor by the 200th quarter-hour measurement. This sensor records the temperature as a near-constant −2 ℃ for approximately 3 weeks. Notice that the 2.5m sensor is also affected by the snow: its diurnal behavior is significantly dampened. Indeed, we can observe that the snow first buries the 1.5m sensor before affecting the 2.5m sensor and that, as the snowpack melts, the 2.5m sensor returns to nominal behavior before the 1.5m sensor. This behavior is consistent with snowpack accumulation and thawing.

In addition to these two sensor malfunctions, there are cases where very infrequent voltage errors can cause effects similar to the sunshield loss. The recorded 15-minute temperature reading at the logger is actually an average of readings taken by the air temperature sensor every 15 seconds. If at any point during the 15 minutes the sensor becomes disconnected or reports out of the voltage range, these bad values can be averaged into a series of good readings, resulting in a mixed error type.

3.1.3 Complex Anomalies

We reserve this classification for anomalies that are so subtle that they cannot be captured without the use of additional sensors. An example of a complex anomaly is a switch in sensor cables between two adjacent sensors on a tower. Because under normal conditions the two sensor readings differ by only a fraction of a degree Celsius, if we examine only one of the sensor streams, we cannot detect the anomaly. However, a model of the joint distribution of all four sensors on the tower should be able to capture the fact that the relative order of the sensor values reflects their physical order on the tower. Specifically, the 4.5m sensor is the hottest of the four in the mid-afternoon and the coolest of the four in the middle of the night. Because the present work only models individual sensor streams, we do not expect it to detect these complex anomalies.

Chapter 4 – Hybrid Bayesian Networks

Our generative model of the air temperature domain is a conditional linear-Gaussian network, also known as a hybrid network due to the presence of both continuous and discrete variables [16, 22]. For the sake of computational convenience, we will only consider continous variables represented by a Gaussian distribution, and only networks where continuous variables have some mixture of discrete and continuous-valued parents and discrete variables have only discrete-valued parents. Discrete variables with continuous-valued parents (represented by a logit distribution) are discussed in further detail in Murphy [23].

4.1 Conditional Gaussian

Consider a single continuous variable, X, represented by the Gaussian distribution $X \sim N\left(\mu, \sigma^2\right)$. For every possible instantiation of values for the discrete parents of X, there is an accompanying parameterization of X; specifically, a separate μ and σ^2. For example, if X has a single boolean parent, $Y = y \in \{true, false\}$, then the conditional probability table (CPT) of X would contain two entries: $P\left(X|Y = true\right) \sim N\left(\mu_t, \sigma_t^2\right)$ and $P\left(X|Y = false\right) \sim N\left(\mu_f, \sigma_f^2\right)$. In general, let $\mathbf{Y} = \{Y_1, Y_2, ..., Y_n\}$ denote the set of discrete parents of the continuous variable X. Further, let $|\mathbf{Y}| = |Y_1| \times |Y_2| \times ... \times |Y_n|$ be the total size (number of possible instantiations) of $\mathbf{Y}$. Then, we specify the CPT of X with the $|\mathbf{Y}|$ dimensional vector, $\vec{\mu} = \langle \mu_1, \mu_2, ..., \mu_{|\mathbf{Y}|} \rangle$. Similarly, we specify the set of possible variances assumable by X, depending on the parent configuration, as the vector $\vec{\sigma^2} = \left\langle \sigma_1^2, \sigma_2^2, ..., \sigma_{|\mathbf{Y}|}^2 \right\rangle$. Figure 4.1 contains an example with binary discrete variables.

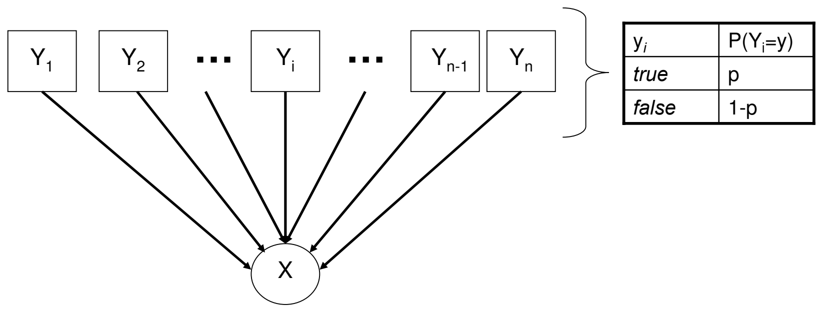

Y_1	Y_2	….	Y_n	μ	σ^2
true	*true*	*true*	*true*	μ_1	σ^2_1
true	*true*	….	*false*	μ_2	σ^2_2
…	…	*false*	*false*	…	…
false	*false*	*false*	*false*	μ_{2n}	σ^2_{2n}

Figure 4.1: Conditional Gaussian Network

4.2 Linear Gaussian

Again, consider a single continous variable, X, parameterized as above. For each continuous-valued parent, $Z_i \in \mathbf{Z} = \{Z_1, Z_2, ..., Z_m\}$, X has an additional regression weight, w_i, such that mean of X is now calculated:

$$\mu_x = \epsilon + \sum_{i=1}^{m} w_i z_i \tag{4.1}$$

where z_i is a value drawn from the Gaussian parent, Z_i, and ϵ is essentially X's constant mean in the linear regression formula. The variance of X is still specified by a single σ^2 parameter and is not conditioned on the parents.

4.3 Conditional Linear-Gaussian

As the name suggests, a conditional Linear-Gaussian (CLG) node is simply a combination of the previous two variable types. Let X be a continuous variable with a set of discrete parents, $\mathbf{Y}$, and continuous parents, $\mathbf{Z}$, as defined above. That is, X has a separate mean, variance, and set of regression weights for each possible instantion of $\mathbf{Y}$. We specify a CLG variable with a mean vector, $\vec{\mu} = \left\langle \mu_1, \mu_2, ..., \mu_{|\mathbf{Y}|} \right\rangle$, a variance vector (again, really just the diagonal of the covariance matrix), $\vec{\sigma^2} = \left\langle \sigma_1^2, \sigma_2^2, ..., \sigma_{|\mathbf{Y}|}^2 \right\rangle$, and a $|\mathbf{Y}| \times |\mathbf{Z}|$ regression matrix:

$$\begin{bmatrix} w_{1,1} & w_{1,2} & \cdots & w_{1,|\mathbf{Z}|} \\ w_{2,1} & w_{2,2} & \cdots & w_{2,|\mathbf{Z}|} \\ w_{...,1} & w_{...,2} & \cdots & w_{...,|\mathbf{Z}|} \\ w_{|\mathbf{Y}|,1} & w_{|\mathbf{Y}|,2} & \cdots & w_{|\mathbf{Y}|,|\mathbf{Z}|} \end{bmatrix} \tag{4.2}$$

Figure 4.2 contains a trivial CLG network with a continuous variable having a single discrete and continuous parent.

y	P(Y=y)
true	p
false	1-p

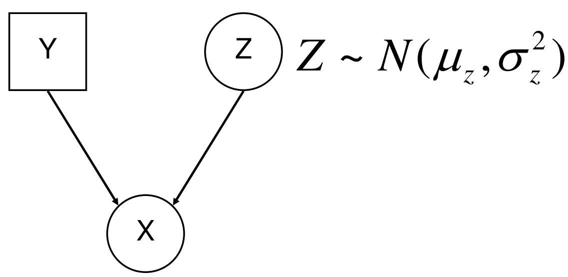

Y	P(X|Y=*y*, Z=*z*)
true	$\sim N(\mu_{1,x} + w_{1,z} * z, \sigma^2_1)$
false	$\sim N(\mu_{2,x} + w_{2,z} * z, \sigma^2_2)$

Figure 4.2: Conditional Linear-Gaussian Network

Chapter 5 – Domain Model

We construct a Conditional Linear Gaussian (CLG) DBN to model the interaction between a single sensor and the air temperature process. Each *slice* of the temporal model represents a fifteen-minute interval, as this is the time granularity of our sensor observations. However, our model also contains two observed discrete variables representing the current time window:

1. $QH = 1, ..., 96$ Representing the current quarter-hour of the day
2. $Day = 1, ..., 365$ Representing the current day of the year.

Thus, every *slice* is associated with a unique $(QH = qh, Day = d)$ pair. The intuition behind this is that, as in the case of the PAR model, we would like to model more rapid or slower fluctuations in temperature depending on periods of the weather cycle (both diurnal and seasonal). Further discussion will be divided into the process model governing air temperature change and the model for sensor behavior.

5.1 The Process Model

For any given time step and (qh, d), we assume the actual temperature, T, is a function of some *learned* baseline value, B (please see section 5.1.1 for discussion of the baseline value) and a value representing the current departure from the baseline value, Δ. That is, we estimate the distribution over T: $T \sim N\left(\Delta + B, \sigma_T^2\right)$.

The Δ variable can be interpreted as representing a temporally local trend effect, such a warm/cold front or a storm. Its purpose is to capture the difference between our baseline expectation for the temperature at a given time of day/day of year and the observed temperature during periods of nominal sensor behavior. We model Δ as a first-order Markov process with the current (qh, d) as additional non-Markovian, observed inputs. Thus, Δ has the distribution $\Delta \sim N\left(\mu_{qh,d} + w\Delta_{t-1}, \sigma^2_{qh,d}\right)$. The Markov process allows the Δ distribution to "wander" in order to capture growing or diminishing trend effects. By conditioning the distribution on QH and D, we can account for sharper temperature shifts associated with particular (qh, d) pairs. For example: the temperature rises and falls more quickly as a result of diurnal effects in summer months than in winter months. To account for this, Δ must be able to change more rapidly (have increased variance) during these periods of the day and season.

5.1.1 Calculating the Baseline

The baseline value for a particular (qh, d) pair estimates the temperature for that time interval after removing short-term trends due to weather systems. Initially, it may seem appropriate to simply average temperature values for a given (qh, d) pair across all of the training years. However, as we have only a few training years, there is too much variance in sample means to provide a good estimate. To

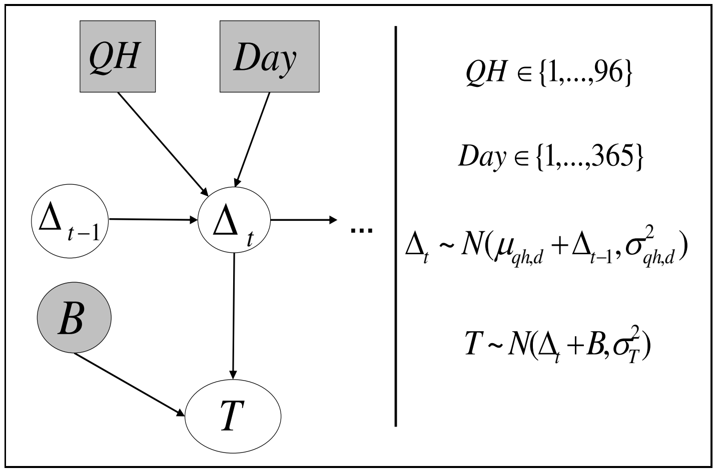

Figure 5.1: Process model for air temperature. Rectangles depict discrete variables, ovals depict normally distributed variables. Shaded variables are observed.

address this, we apply a moving average kernel smoother across the M days on either side of the current day and the N quarter-hour periods on either side of the current quarter hour. However, if we only used this simple smoother, it would be biased low at times when the second derivative of the temperature was negative (at the point of maximum temperature) and biased high at times when the second derivative of the temperature was positive. To correct for this, we compute the first derivative $Q(d, qh, t, y)$ for each (u, t) offset, and use this to remove the short-term linear trend in the temperature curve:

$$B_{qh,d} = c \sum_{y,u,t} T(d+u, qh+t, y) - Q(d, qh, t, y) \quad (5.1)$$

$$c = \left[Y(2M+1)(2N+1)\right]^{-1} \quad (5.2)$$

where $y \in \{1, ..., Y\}$ denotes the year index, $u \in \{-M, ..., M\}$ denotes the day offset, $t \in \{-N, ..., N\}$ denotes the quarter-hour offset, and $T(d, qh, y)$ is the training value for a given (d, qh, y) tuple.

$Q(d, qh, t, y)$ is the first-derivative offset function that calculates the average deviation from the current quarter-hour to t over a $2M + 1$ day window. It is calculated as:

$$Q(d, qh, t, y) = (2M + 1)^{-1} \sum_{u} T(d + u, qh + t, y) - T(d + u, qh, y). \quad (5.3)$$

Figure 5.2 shows this algorithm applied to a week-long sliding window in the calculuation of a single point of the baseline (note that this value would then be averaged across all training years instead of the single year shown).

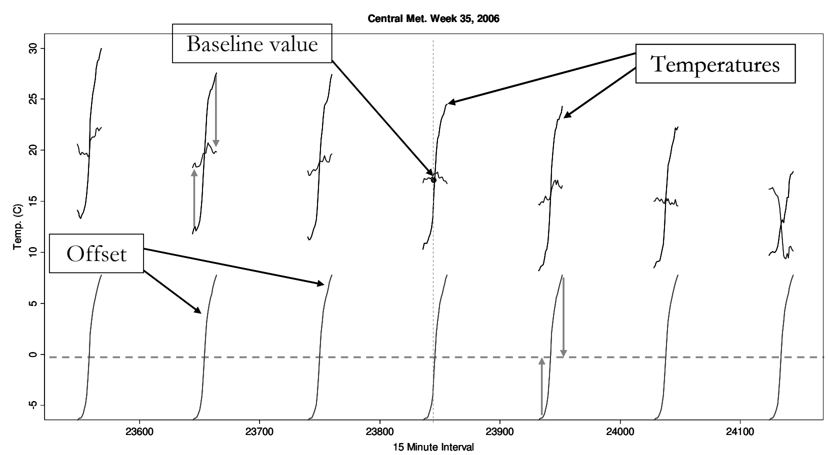

Figure 5.2: Computation of Baseline Value over Week-long Window.

The offset for the $2N + 1$ length quarter-hour window is first calculated by taking the difference between each quarter-hour in that window and the current

(qh, d) value for which we are calculating the baseline, and then averaging that difference across all days in the $2M + 1$ day window. This offset will be centered around 0, as indicated in the figure. Next, we subtract this offset value (which will be the same across all $2M + 1$ days) from the observed values in our window. The result of this is the detrended data should resemble a relatively flat segment for each day in the window (shown in the figure as intersecting with the training data). The baseline value is then calculated as the average of all detrended values for the day and quarter-hour window.

5.2 Sensor Model

Based on our discussions with the expert, we have identified several anomaly types in the temperature data streams. However, we are not confident that we have found all anomaly types. Each time we meet with the expert, we learn about a new anomaly, and there is no reason to expect that the set of anomalies is fixed. Hence, rather than attempting to model each type of anomaly separately, which would lead to a system that could only recognize a fixed set of anomaly types, we decided to develop a single, very general fault model that is able to capture most of the known anomaly types and (we hope) unknown types as well. We model the state of the sensor, S, as a discrete variable that summarizes the degree of sensor functionality. We chose four levels of sensor quality at the behest of the domain expert to discriminate between slightly erroneous values (which may still have some use) and truly erroneous values. The state S is modeled as a first-order Markov process, which allows us to capture the fact that good sensors tend to stay good and bad sensors tend to stay bad. The observed temperature, O, is distributed as $N(\mu_s + w_s T, \sigma_s^2)$, where the values of σ_s^2 capture how well the observed temperature is tracking the true temperature as a function of the current state $S = s$. Figure 5.3 depicts the full domain model.

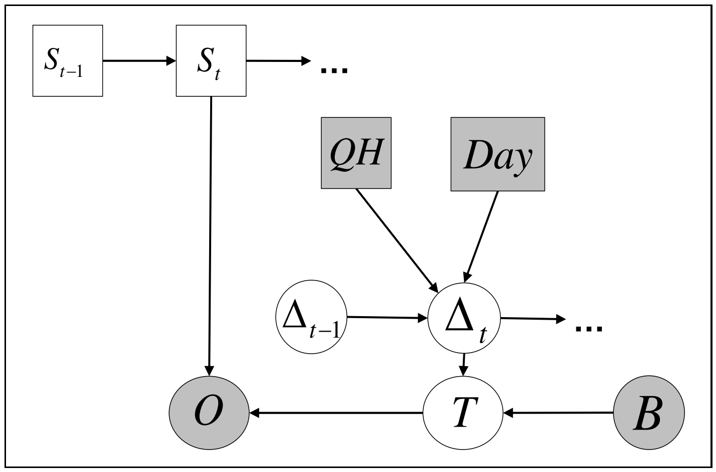

Figure 5.3: Integrated single-sensor and process model.

Chapter 6 – Methods

We obtained eleven years of raw air temperature from the H. J. Andrews Experimental Forest (1996 - 2006). This data had been processed by the domain expert to mark all anomalous data points. The domain expert has a tendency to overlabel data; a long time interval may be labeled as anomalous even though it contains some short time intervals where the data is not anomalous. This behavior is predominately observed on medium-type anomalies, where it can be difficult to discern isolated anomalies at the 15-minute time granularity. For example, if a sun shield was missing, the expert would mark the entire time interval when the shield was missing as anomalous even though at night time and on cloudy days the temperature readings are accurate.

6.1 Model Parameterization

For each of the three meteorological stations, we selected four years of data as our training set. From this set, we removed all data points labeled anomalous by the expert and trained on the remaining data. We calculated a baseline value for every (qh, d) pair as described in section 5.1.1, with the number of days $M = 3$ and the number of quarter hours $N = 5$. Using these values, we then iterated through the training set and calculated the following:

$$\Delta(y, d, qh) \quad = \quad T(y, d, qh) - B(d, qh), \tag{6.1}$$

where $T(y, d, qh)$ is the recorded temperature for that year, day, and quarter-hour, and $B(d, qh)$ is the baseline value.

To fit the conditional distribution for Δ, we smooth over a 31-day window. We compute the mean and variance of $\Delta_{qh,d}$ as

$$\mu_{qh,d} = (YM)^{-1} \sum_{y,u} \Delta(y, d+u, qh) - \Delta(y, d+u, qh-1) \tag{6.2}$$

$$\sigma^2_{qh,d} = (YM)^{-1} \sum_{y,u} (\Delta(y, d+u, qh) - \mu_{qh,d})^2 \tag{6.3}$$

where $Y = 4$ is the number of years, and $M = 31$ is the number of days.

We manually tuned the parameters for the predicted temperature (T), the observed temperature (O), and the sensor (S) variables to implement the generic fault model. The sensor can be in one of four states: {Very Good, Good, Bad, Very Bad}. The first three states assert equality between the mean of the predicted and observed temperatures, and the last state encompasses anomalies in which the observed temperature is completely independent of T. We impose this artificial gradient of sensor qualities so that end users can make a more informed choice with regards to the data quality they wish to use. That is, a binary labeling system {Good, Bad} may dissuade a user from using any data labeled *Bad* even though the degree of error may be trivial, as in the case of sensor-swapped data.

Table 6.1: Observed Temperature as a function of Sensor State and Predicted Temperature

SENSOR STATE	DISTRIBUTION
$O \mid S_t = VeryGood$	$N(T, 1.0)$
$O \mid S_t = Good$	$N(T, 5.0)$
$O \mid S_t = Bad$	$N(T, 10.0)$
$O \mid S_t = VeryBad$	$N(0, 100000)$

We calculate the actual temperature as the sum of the baseline and the current Δ offset. We assign weights of 1.0 for both these variables and set Δ's mean to 0. Further, we supply Δ with a very low, non-zero variance. The distribution over the observed temperature is tied to the state of the sensor, and thus we can use the sensor state to explain large residuals between the observed and predicted temperature. In cases where the sensor is believed to be functioning nominally, the observed temperature should be the predicted temperature with some minimal variance. If we believe the sensor is malfunctioning, we allow the observed temperature to take on additional variance yet still reflect the mean of the predicted temperature. In cases where we believe the sensor is completely failing, we set the weight from the predicted temperature to 0, and we assign a huge variance to O. Table 6.1 displays the distribution of O given the state of S.

6.2 Model Simulation

We perform inference in our network using a variation on the Forward Algorithm [26, 29] and Bucket Elimination adapted for CLG networks [7, 8, 15]. The Forward Algorithm computes the marginal for every step of a Markov process and passes that distribution forward as the *alpha message*. The Bucket Elimination algorithm is a dynamic-programming, exact-inference method that represents potentials as buckets and marginalizes out variables iteratively until only the desired potential remains.

Table 6.2 outlines our modified Forward inference method. The two modifications to the Forward algorithm occur in steps 3 and 5. In 3, we enforce a decision about the state of the sensor and use its most likely value to constrain the distribution on Δ computed in 4. In other words, at each step, we compute the posterior distribution over S and then force S to take on its most likely value. This is necessary to prevent the variance associated with Δ from growing rapidly.

Consider the elimination ordering in Table 6.3. The potential in (1) will fail to sufficiently constrain the variance of Δ_t, because there is always a non-zero probability that $S_t =$ Very Bad. The high variance associated with the general fault state of the sensor then removes the constraining effect the observation O provides. By entering evidence for the sensor state before computing the posterior of Δ_t, we eliminate this problem. The additional observation for S_t changes the expression in (1) to:

$$P(O = o|S_t = s, T)P(T|B = b, \Delta_t) = Pot(\Delta_t) \tag{6.4}$$

Table 6.2: Modified Forward Algorithm

1. Enter evidence for observed variables: QH, Day, B, and O
2. Compute the posterior for S_t as the new alpha message, α_S
3. Enter the most likely value of S_t, $\underset{s}{\operatorname{argmax}} P\left(S_t = s \mid O_{1:t}\right)$ for time t and as additional evidence.
4. Compute posterior for Δ_t as the new alpha message, α_Δ
5. If $s =$ Very Bad, then set variance of α_Δ to $\min\left(\sigma^2_{qh,d}, \sigma^2_x\right)$ where $\sigma^2_{qh,d}$ is the regular variance of Δ for that (qh, d) pair and σ^2_x is the calculated variance of α_Δ
6. Update S_{t-1} to α_Q and Δ_{t-1} to α_Δ (pass α messages forward) and return to 1.

and removes the potential calculated in (4). $Pot(\Delta_t)$ sufficiently constrains Δ_t's variance for all values of s_t except *Very Bad*. We address the latter case in step 5 of our algorithm (Table 6.2) by setting an upper limit on the variance of the posterior. The limit is the trained variance parameter for Δ for the current (qh, d) pair.

6.3 Inference in CLG Networks

As mentioned in 6.2, we perform exact inference in our model using a Variable/Bucket Elimination algorithm adapted to CLG networks. We outline the inference process in hybrid networks here; however, we refer the reader to Lau-

Table 6.3: Bucket Elimination for $P(\Delta_t)$ Elimination Ordering: T, Δ_t, S_t, S

$$P(O = o|S_t, T)\,P(T|B = b, \Delta_t) = Pot(\Delta_t|S_t) \tag{6.5}$$
$$P(\Delta_t|\Delta_{t-1})\,P(\Delta_{t-1}) = Pot(\Delta_t) \tag{6.6}$$
$$P(S_t|S_{t-1})\,P(S_{t-1}) = Pot(S_t) \tag{6.7}$$
$$Pot(\Delta_t|S_t)\,Pot(S_t) = Pot(\Delta_t)' \tag{6.8}$$
$$Pot(\Delta_t)\,Pot(\Delta_t)' \tag{6.9}$$

ritzen and Murphy [15, 16, 22] for a more thorough explanation.

Recall that in Variable Elimination, first an elimination ordering is determined either at random (as in our case) or in such a way as to minimize the induced width of any potential (a known NP-Hard problem, [2]). The algorithm then iterates through each variable in the elimination list. For each iteration, the algorithm combines all variables related to the current variable in the list into a bucket by taking the pointwise product of all variables' CPTs and then eliminates the current variable through marginalization. We will refer to merged CPTs in a bucket as a potential, denoted $Pot(x_1, x_2, ..., x_n)$, where $x_1, x_2, ..., x_n$ refers to the variables in the bucket.

Prior to any computation, we first represent each variable's CPT in terms of its canonical characteristics, $g, \mathbf{h}$, and K. For the Normal distribution (univariate case), these characteristics are computed from the CLG parameters (section 4.3) as the following:

$$g = -\frac{\mu^2}{2\sigma^2} - \frac{1}{2}\log\left(2\pi\sigma^2\right) \tag{6.10}$$

$$\mathbf{h} = \frac{\mu}{\sigma^2}\begin{bmatrix} -\mathbf{w} \\ 1 \end{bmatrix} \tag{6.11}$$

$$K = \frac{1}{\sigma^2}\begin{bmatrix} \mathbf{w}\mathbf{w}^T & -\mathbf{w} \\ -\mathbf{w}^T & 1 \end{bmatrix} \tag{6.12}$$

Note that $\mathbf{w}$ is a vector of weights associated with the LG or CLG variable, so $\mathbf{h}$ will be a vector of size of $|\mathbf{w}|+1$ and K will be a $(|\mathbf{w}|+1)\times(|\mathbf{w}|+1)$ matrix.

For the discrete variables, we replace each entry in the variable's CPT with the canonical formulation of its probability, which is simply $g = \log p$ where p is probability value. $\mathbf{h}$ and K are initialized as an empty vector and matrix, respectively.

6.3.1 Product & Marginalization

Once all CPTs are represented by their canoncial characeristics, multiplying two CPTs is a two-step process. Let us consider the product between two CPTs (or potentials), denoted ϕ_1 and ϕ_2, over the sets of variables $\{x_1, x_2, ..., x_n\}$ and $\{y_1, y_2, ..., y_m\}$, respectively. Recall that the resultant pointwise product of $\phi_1 \times \phi_2$ will be a potential over the union of the variables in ϕ_1 and ϕ_2, $\{x_1, ..., x_n, y_1, ..., y_m\}$. Thus, our first step is to extend the domain of the canonical characteristics of ϕ_1

and ϕ_2 such that they now include all variables in the aforementioned union. This is done by inserting rows or columns of zeros into the $\mathbf{h}$ and K components accordingly. Next, the product of ϕ_1 and ϕ_2 is then simply computed as:

$$(g_1, \mathbf{h}_1, K_1) * (g_2, \mathbf{h}_2, K_2) = (g_1 + g_2, \mathbf{h}_1 + \mathbf{h}_2, K_1 + K_2). \tag{6.13}$$

Once all CPTs in a bucket have been multiplied, the current variable in the elimination ordering must be marginalized from the potential. If the variable being marginalized is continuous-valued, this is done by first breaking the $\mathbf{h}$ and K canonical components of the potential into distinct sections as follows:

$$\mathbf{h} = \begin{pmatrix} \mathbf{h}_1 \\ \mathbf{h}_2 \end{pmatrix} \tag{6.14}$$

$$K = \begin{pmatrix} K_{11} & K_{12} \\ K_{21} & K_{22} \end{pmatrix} \tag{6.15}$$

where $\mathbf{h}_1$ refers to the index of the variable to-be-eliminated in the list of continuous variables in the potential, and $\mathbf{h}_2$ denotes the remaining continuous variables. Similarly, K_{11} refers to the row and column index of the variable to-be-eliminated in the K matrix, K_{12} is the K matrix minus the column containing the variable, K_{21} is the matrix minus the row containing the variable, and K_{22} is the K matrix minus both the row and column containing the variable. Finally, the new canonical characteristics representing the marginalized potential are calculated as follows:

$$\hat{g} = g + \frac{1}{2}\left(p\log(2\pi) - \log|K_{11}| + \mathbf{h}_1^T K_{11}^{-1}\mathbf{h}_1\right) \quad (6.16)$$

$$\hat{\mathbf{h}} = \mathbf{h}_2 - K_{21}K_{11}^{-1}\mathbf{h}_1 \quad (6.17)$$

$$\hat{K} = K_{22} - K_{21}K_{11}^{-1}K_{12} \quad (6.18)$$

where p is the dimension or length of the vector $\mathbf{h}_1$. In the case of marginalizing a discrete variable, we approximate the mixture of Gaussians by reducing the mixture into a single component. This process is done with the moment form of the potential:

$$\hat{p}(i) = \sum_j p(i,j) \quad (6.19)$$

$$\hat{\mu}(i) = \sum_j \mu(i,j)\, p(i,j)\,/\hat{p}(i) \quad (6.20)$$

$$\hat{\Sigma}(i) = \sum_j \Sigma(i,j)\, p(i,j)\,/\hat{p}(i) + \quad (6.21)$$

$$\sum_j \left(\mu(i,j) - \hat{\mu}(i)\right)\left(\mu(i,j) - \hat{\mu}(i)\right)^T p(i,j)\,/\hat{p}(i), \quad (6.22)$$

where j refers to instantations of the discrete variable being summed out. Because the inverse of the product of two covariance matrices may not always be well-defined, we avoid working in the moment form until absolutely necessary. We do this by enforcing a strong triangulation [14] elimination ordering that always eliminates continuous-valued variables before discrete. This insures that when we do perform margninalization over a discrete variable, all products involving

Gaussian variables have already been performed.

Chapter 7 – Results

We evaluate our method over seven years of labeled data from the H.J. Andrews while holding out four years for training. Training and testing years were individually selected for each site with a preference for years including few or no anomalies in the training set, and years exhibiting the largest diversity of anomaly types in the test set. We analyze our results in terms of anomaly difficulty and then introduce an additional classification method designed to approximate the behavior of the domain expert. Finally, we report overall precision and recall with regard to our classification system and each meteorological station.

7.1 Simple Anomaly Types

Figure 7.1 shows a typical result provided by the model for intermittent sensor faults associated with a voltage error in the sensor. Plotted points indicate points labeled as anomalous (Bad or Very Bad) by our system. We omit the *Good* and *Very Good* labels for clarity. Note that all values of -6999.9 ℃ were correctly labeled as *Very Bad*; also, the model produced no false positives for the week shown. The predicted temperature values inserted (the dotted line) in place of those labeled anomalous closely resemble the neighboring valid segments of the data stream.

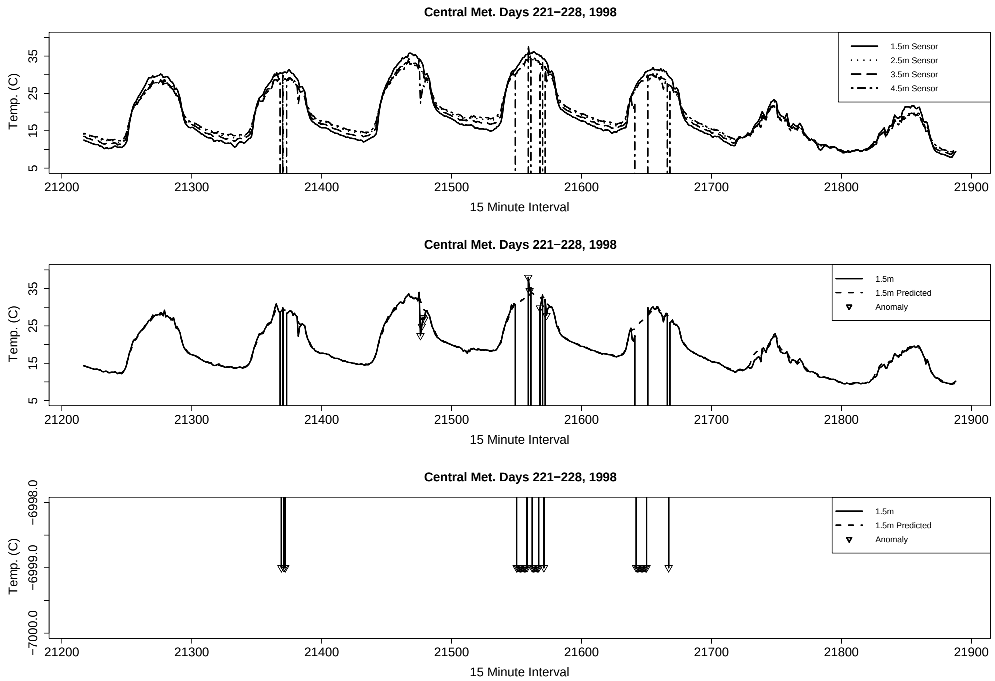

Figure 7.1: Top: Original data stream containing a faulty 4.5m sensor. Center & Bottom: Data cleaning results for the 4.5m sensor.

7.2 Medium Anomaly Types

Let us consider the broken sun shield anomaly introduced in Section 2.2.2. Figure 7.2 (bottom) shows the labeling provided by our method on an anomalous section of data. The model correctly identifies the ascending and descending segments of the day as anomalous, while labeling those periods unaffected by the broken sun shield (night time and periods of cloud cover) as normal. On some days, the model correctly labels the peak of the diurnal period as anomalous, but in other cases (e.g., t=4100), it does not. This is because the short-term behavior at the peak looks normal (except for its absolute value): the temperature reaches its high for the day, it holds steady for a short period, and then begins to decrease. The reduced rate of change in temperature between time slices then falls within the range of Δ's variance, so it is labeled as non-anomalous. Note that the model-predicted temperature slightly lags the observed 4.5m temperature. This matches the 1.5m, 2.5m, and 3.5m sensors, which are labeled by the domain expert as functioning nominally for this period and corrects for the incorrect acceleration/deceleration introduced by the fault.

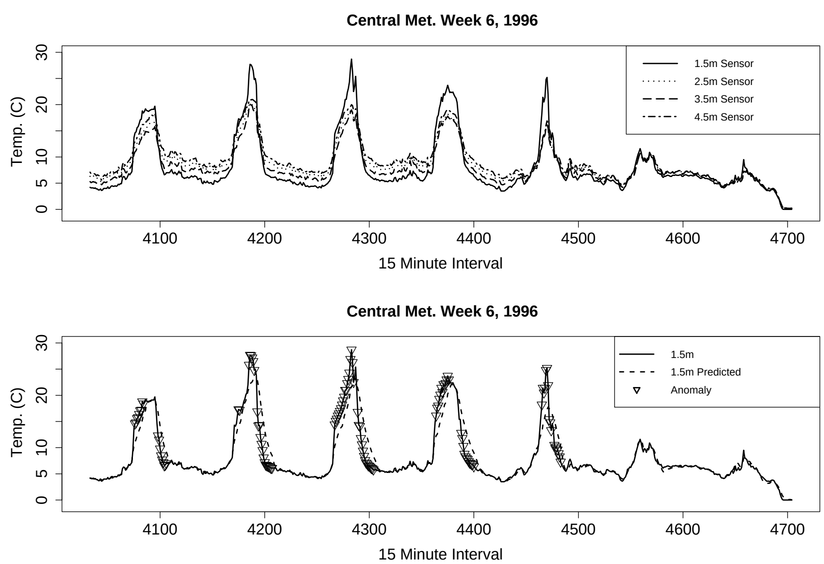

Figure 7.2: Top: Lost sun shield in 1.5m sensor. Bottom: Data cleaning applied to 1.5m sensor.

7.3 Class Widening

As a result of working at very fine time granularities, the domain expert tends to "over-label" faults (i.e., marking long segments as faulty even though only some of the points in those segments are actually faulty). We correct for this behavior when directly comparing our classification to the expert's by introducing a widening method. For any point labeled as anomalous (Bad or Very Bad) by both the expert and our system, we widen our classification by assigning the same class to λ points before and after the current quarter hour. We apply this widening only to those anomalous types we consider to be non-trivial, as the expert is very precise in labeling of extreme anomalies (out of voltage range, sensor disconnects, etc.).

7.4 Precision and Recall

Figure 7.3 displays the precision and recall results for each of the meteorological stations over a range of λ values for the aforementioned widening method. The diamond-marked line represents the average performance among all three sites. The benefit gained from the application of class widening is largely dependent on the types of anomalies encountered at each site. For example, the Central Met station benefits the most from widening because that site contained many medium-type anomalies (broken sun-shield predominately), which tend to be over-labeled in manual inspections. The class widening method allows us to tune our system to simulate the domain expert labeling (obtain higher recall rates) at the cost of our false positive rate. For example, by increasing λ from 0 (individual labeling) to 200 (2-day window on either side of the current quarter hour), we have increased our average recall from 61% to 78%; however, we have done so at the cost of increasing our false positive rate from 2.1% to 3.2%. Our results indicate that $\lambda = 70$ provides the highest precision score before beginning to decline as a result of increased false positives rates. At this λ value, we achieve an average precision, recall, and FPR across all testing sets of 38%, 73%, and 2.5%, respectively. However, these overall numbers hide many different situations, so we will analyze our results with respect to the precision and recall values obtained at each meteorological station.

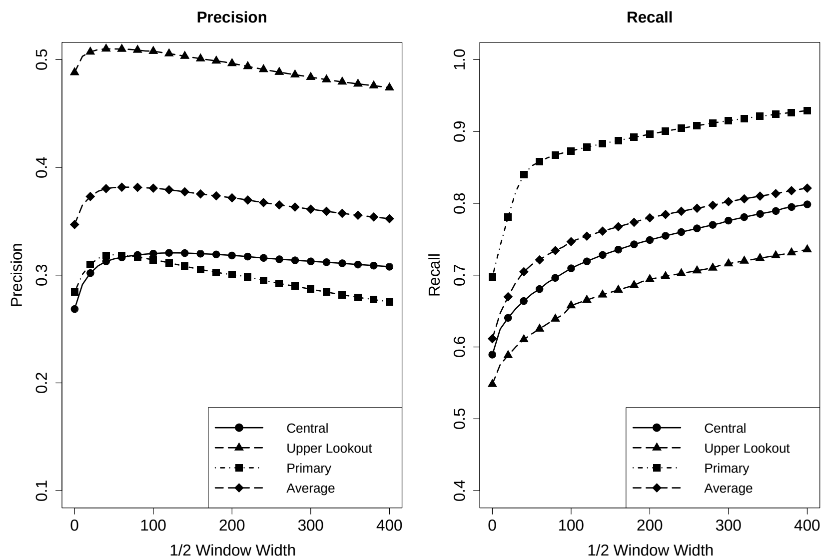

Figure 7.3: Precision and Recall as a function of λ. Marked increments of 100.

7.5 Central Meteorological Station

Figure 7.4 displays a scattergram of the results of our classification method ($\lambda = 70$) applied to the Central Met test sets. The comma-separated values below each circle relate the sensor (1, 2, 3, and 4 referring to the 1.5m, 2.5m, 3.5m, and 4.5m sensors) and test year (1996, 1997, 1998, 2001, 2002, 2003, 2004).

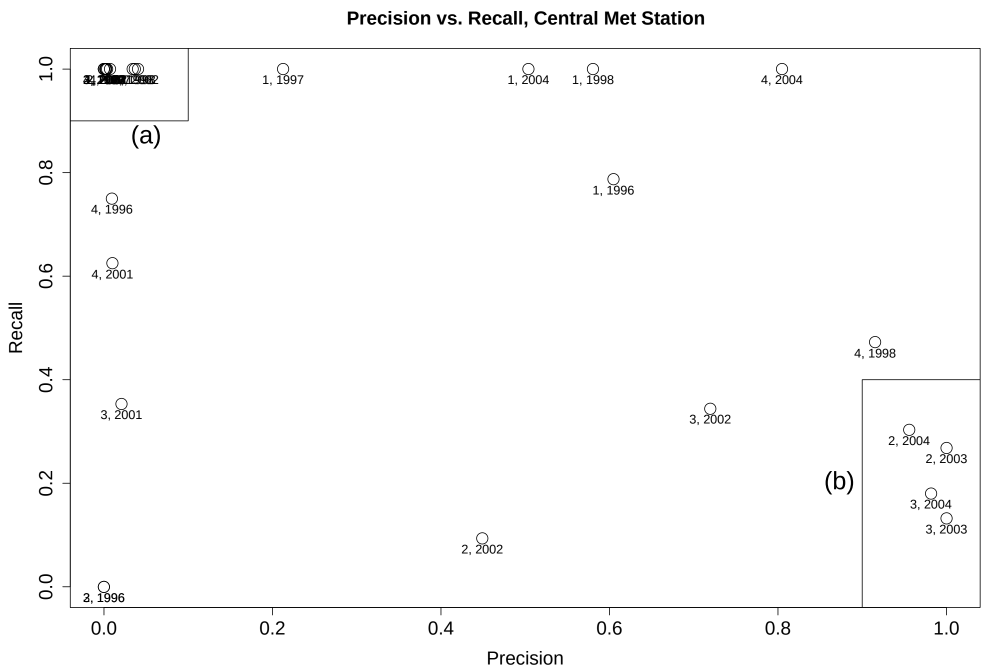

Figure 7.4: (a) Infrequent, simple anomalies and (b) long-term sensor swaps.

The region denoted as (a) contains years having infrequent, short-duration, simple anomalies. 11 of the 28 data sets from Central Met fall into this category. They contain very few actual anomalies (median = 3), which are easily detected by system (recall rates of 100% are obtained on these data sets). Unfortunately, because these anomalies are so sparse, our precision rate is adversely affected by our false positive rate. Even our modest false positive rate of 1.9% (approximately 666 FP's per 35040 values in a data set) dominates our precision score. These numbers are still very good. Our goal is to produce a system that can be used as a filter to focus the time and attention of the domain expert on those points most likely to be anomalous. Consequently, if the expert examines all of the points that we predict to be positive, this will reduce by 98% the number of points that must be examined while still detecting all true anomalies. As we move right across the x-axis, we see our precision rates improve on data sets that contain more frequent simple anomaly types.

As we move down the y-axis from (a), we come across data sets that still contain few anomalies, but the anomaly type is less clear. In the extreme case, the 2.5m and 3.5m sensors from Central 1996 both contain a single labeled anomaly that appears entirely consistent with neighboring values, and is misclassified by our system. The region in (b) contains data sets almost entirely dominated by anomalous values (median = 30565.5); these are probably values expunged from the database due to swapped sensor leads. We obtain high precision on these sets because essentially any value we classify as anomalous was labeled as such by the expert. Similarly, our poor recall scores on these sets is a result of the fact that much of the data looks completely normal, and our system is as-of-yet unable to detect swapped sensor leads. The remaining data sets populating the scatterplot represent a trade off between the two regions denoted in (a) and (b). That is, they tend to be data sets containing medium anomaly types (sun shield failures, voltage-range errors) of increasing duration as we move right across the x-axis and more obvious as we move up the y-axis.

Tables 7.1 and 7.2 contain anomaly counts and accuracy scores (percent of points classified by our system correctly) for each data set at the Central Met station using our class-widening technique with $\lambda = 70$. With the exception of the 4 data sets denoted in (b), we tend to achieve fairly high accuracy scores.

Year	1.5m	2.5m	3.5m	4.5m
1996	2537.0	1.0	1.0	4.0
1997	302.0	0.0	0.0	2.0
1998	984.0	13.0	13.0	4420.0
2001	3.0	3.0	68.0	8.0
2002	3.0	5512.0	5890.0	19.0
2003	2.0	35040.0	35040.0	0.0
2004	1369.0	26091.0	26091.0	1369.0

Table 7.1: Anomaly Counts for Central Met sensors

Year	1.5m	2.5m	3.5m	4.5m
1996	0.9473	0.9860	0.9804	0.9909
1997	0.9680	0.9858	0.9829	0.9920
1998	0.9797	0.9895	0.9902	0.9279
2001	0.9656	0.9769	0.9664	0.9859
2002	0.9660	0.8393	0.8672	0.9871
2003	0.9602	0.2678	0.1322	0.9953
2004	0.9615	0.4706	0.3871	0.9905

Table 7.2: Accuracy scores for Central Met sensors

Moreover, we maintain low false-positive rates for the data sets while achieving an average recall of 69% (the sets in (b) taken into account).

7.6 Primary Meteorological Station

Figure 7.5 displays a scattergram of the results of our classification method ($\lambda = 70$) applied to the Primary Met test sets. As in figure 7.4, the comma separated values detail the sensor and year of the test set. Note that the labels have been omitted from the sets in (a) for the sake of clarity.

The region in (a) represents the set of test sets similar to those in Figure 7.4 (a);

Year	1.5m	2.5m	3.5m	4.5m
1996	0.0401	0.0139	0.0195	0.0089
1997	0.0321	0.0141	0.0170	0.0079
1998	0.0208	0.0104	0.0097	0.0063
2001	0.0343	0.0230	0.0323	0.0139
2002	0.0339	0.0214	0.0270	0.0129
2003	0.0397	0.0	0.0	0.0046
2004	0.0400	0.0408	0.0098	0.0098

Table 7.3: False positive rates for Central Met sensors

that is, years containing infrequent, short-term anomalies that are of the simple type. There are 13 such data sets in the Primary Met station with a median anomaly count of 74, in which we obtain precision scores $\leq .2$ and recall scores $\geq .8$. The data sets enclosed in (b) contain a mixture of simple anomaly types like those in (a), some short periods of sensor disconnects, as well as several voltage-related anomaly types. Our precision scores increase on these 10 data sets for many of the same reasons they increased on the Central Met sets; the anomaly types are easily detected by our system, and the abundance of these anomalies (median=626) begins to compensate for our false-postive rate. Finally, the four sets from sensors 3 and 4 for years 2003 and 2004 contain sensor swaps, resulting in higher precision scores and, ufortunately, reduced recall. Tables 7.4, 7.5, and 7.6 display the anomaly counts, accuracy scores, and false positive scores for the Primary Met testing sets.

Year	1.5m	2.5m	3.5m	4.5m
1998	721.0	626.0	626.0	626.0
2000	569.0	474.0	472.0	1153.0
2001	149.0	70.0	70.0	70.0
2002	1.0	11016.0	11016.0	1.0
2003	10.0	17914.0	35040.0	11.0
2004	100.0	99.0	4282.0	100.0
2006	1456.0	154.0	154.0	584.0

Table 7.4: Anomaly Counts for Primary Met sensors

Year	1.5m	2.5m	3.5m	4.5m
1998	0.9793	0.9813	0.9803	0.9805
2000	0.9662	0.9705	0.9723	0.9715
2001	0.9723	0.9767	0.9726	0.9683
2002	0.9702	0.7547	0.7690	0.9684
2003	0.9816	0.6258	0.1898	0.9731
2004	0.9686	0.9718	0.8630	0.9680
2006	0.9580	0.9561	0.9612	0.9698

Table 7.5: Accuracy scores for Primary Met sensors

Year	1.5m	2.5m	3.5m	4.5m
1998	0.0206	0.0188	0.0197	0.0195
2000	0.0342	0.0298	0.0280	0.0294
2001	0.0276	0.0233	0.0273	0.0317
2002	0.0297	0.0455	0.0496	0.0315
2003	0.0183	0.0188	0.0	0.0268
2004	0.0314	0.0281	0.0295	0.0319
2006	0.0437	0.0440	0.0389	0.0306

Table 7.6: False positive rates for Primary Met sensors

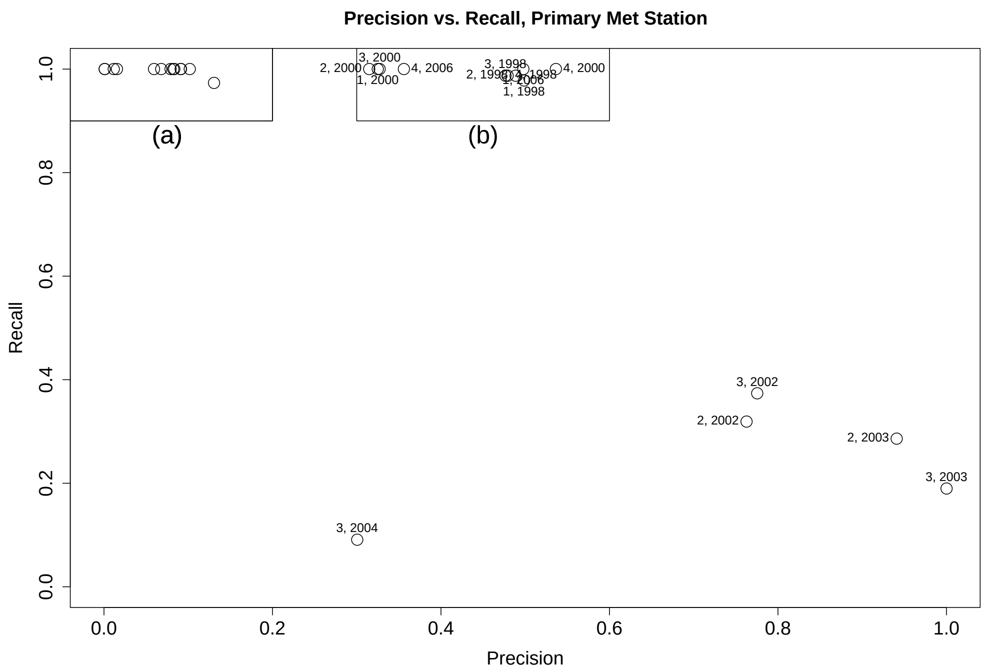

Figure 7.5: (a) Infrequent, simple anomalies and (b) semi-frequent simple & medium anomalies.

7.7 Upper Lookout Meteorological Station

Figure 7.6 displays a scattergram of the results of our classification method ($\lambda = 70$) applied to the Upper Lookout Met test sets. As in the previous two scattergrams, the comma separated values detail the sensor and year of the test set. Again, the labels have been omitted from the sets in (a) for the sake of clarity. The section in (a) represents those data sets (8 in total) with few (median = 6), easily detected anomalies.

Upper Lookout, located at the highest altitude of the three stations, often receives enough cumulative snowfall to damage low-lying sensors on the tower

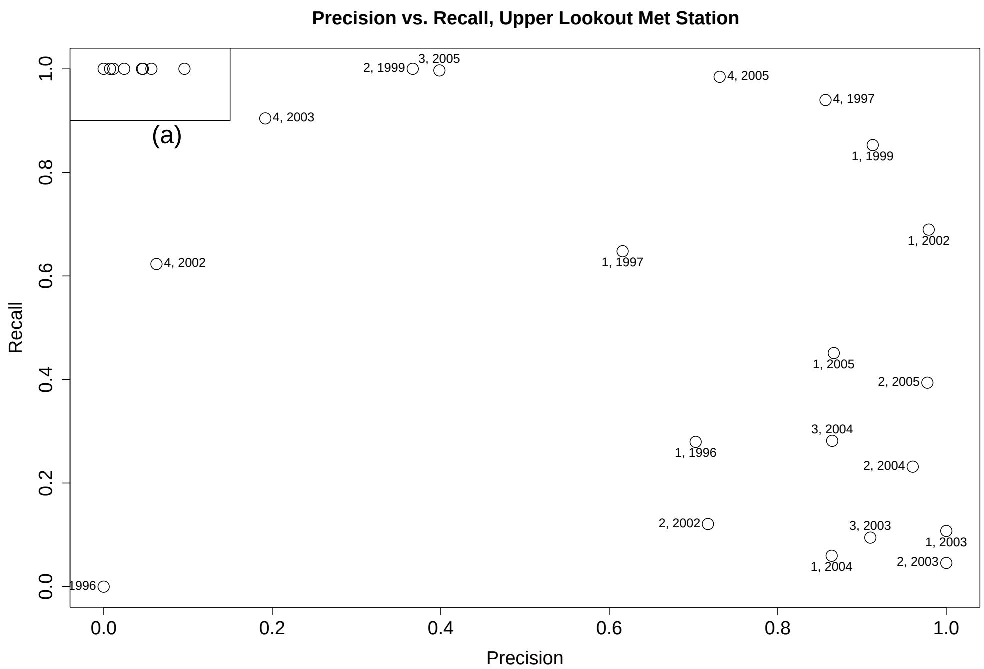

Figure 7.6: (a) Infrequent, simple anomalies.

(1.5m & 2.5m). In section 3.1.2, we displayed an example of the sensor's behavior during a significant snowpack. In response to this, the 1.5m and 2.5m sensors are sometimes disconnected for extended periods (-53.3 ℃ recorded) of time ranging from early fall to late spring. Within the test set, this practice can be seen during years 1999, 2002, and late 2005 (beginning in December) for the 1.5m sensor. Results for the former two years reflect this very long-duration, simple anomaly as being very easy to detect. We obtain relatively high precision ($\geq .6$) and recall ($\geq .6$) for these data sets. For 2005, our system obtains a lower recall rate because it appears the 1.5m sensor is labeled anomalous by the domain expert well before it is actually disconnected, though while it is still reporting (what appear to be in the context of neighboring, functional sensors) valid temperatures. The 2.5m and 3.5m sensors during 2003 and 2004 display a mixture of sensor disconnects (in the case of the 2.5m sensor) and sensors swaps (between the 2.5m and 3.5m sensor), resulting in higher precision and lower recall. For years where the 1.5m sensor is left to endure the winter (1996, for example), our system fails to accurately detect the snow burial of the sensor. This is because a temperature reading of 0 ℃ is not particularly abnormal for this site during the winter months, and diurnal variation is normally suppressed during that time of year. The Δ variable begins to compensate for the lack of any diurnal variation, and the snow burial is, in effect, handled as a long-term storm period would be at other sites.

Tables 7.7, 7.8, and 7.9 display the anomaly counts, accuracy scores, and false-positive rates for each of the Upper Lookout test sets. The unusually high false positive rate associated with the 1.5m sensor during the 1999 year is related to an unfortunate side-effect of our classification scheme. The 1999 year contains a prolonged sensor disconnect period, which is trivial for our system to detect. However, the Δ variable in our network attempts to compensate for the constant value being reported by the sensor by slowly drifting its mean towards that value (as fast as the capped variance will allow). This means that when the sensor is reconnected and starts behaving normally immediately after a long period of anomalous behavior (mid-February to November), our system has to adjust for this change. This rate of adjustment will vary proportionately to the length of the error and the magnitude of the anomalous value. During this readjustment period, the system will flag all normal values reported from the sensor as anomalous until such time as the predicted distribution converges to the observed temperature.

Year	1.5m	2.5m	3.5m	4.5m
1996	3470.0	1400.0	0.0	13.0
1997	1456.0	5.0	6.0	1265.0
1999	29300.0	88.0	9.0	14.0
2002	26565.0	7797.0	3.0	321.0
2003	35040.0	35040.0	9475.0	334.0
2004	16183.0	19449.0	4386.0	2.0
2005	8716.0	7864.0	681.0	1450.0

Table 7.7: Anomaly Counts for Upper Lookout Met sensors

Year	1.5m	2.5m	3.5m	4.5m
1996	0.9169	0.9549	0.9962	0.9922
1997	0.9685	0.9942	0.9964	0.9921
1999	0.8085	0.9956	0.9975	0.9933
2002	0.7537	0.7937	0.9925	0.9111
2003	0.1071	0.0456	0.7526	0.9627
2004	0.5612	0.5680	0.9045	0.9924
2005	0.8461	0.8619	0.9706	0.9843

Table 7.8: Accuracy Scores for Upper Lookout Met sensors

Year	1.5m	2.5m	3.5m	4.5m
1996	0.0129	0.0053	0.0037	0.0077
1997	0.0175	0.0057	0.0035	0.0058
1999	0.4163	0.0043	0.0024	0.0066
2002	0.0455	0.0136	0.0074	0.0862
2003	0.0	0.0	0.0034	0.0367
2004	0.0080	0.0119	0.0062	0.0075
2005	0.0230	0.0026	0.0298	0.0156

Table 7.9: False positive rates for Upper Lookout Met sensors

Chapter 8 – Conclusions

This research has demonstrated a practical application of hybrid Dynamic Bayesian Networks to the problem of anomaly detection. Our network incorporated a baseline function to estimate an "average" temperature for a given day and quarter-hour, as well as a Markovian Δ-component to capture local deviations from the baseline caused by storm effects. We provided a demonstration of exact inference in our network using Variable Elimination (adapted to Conditional Linear Gaussian variables) and Forward inference.

Our anomaly detection system was tested against seven years of air temperature data from each of the three sites: Primary, Upper Lookout, and Central Meteorological stations. The experimental results show that we are able to detect all simple anomaly types (voltage range and sensor disconnects) present in the data. Moreover, our system has proven capable of detecting some medium-difficulty anomaly types, including sun shield failures and more subtle voltage issues (see Section 3.1.2). In order to compensate for the discrepancy between our labeling method and that practiced by the domain expert, we introduced a class-widening scheme, which approximated the pattern of "over-labeling" of medium and complex difficulty anomalies. Our ability to capture to all simple anomalies present in the data is reflected in our high recall rates on these data sets. Unfortunately, these high recall scores are typically coupled with low precision values due to the sparseness of these simple anomaly types in most data sets. That is, the most common data sets found at all three sites were those containing very few, simple anomaly types. Thus, while our overall false positive rate is fairly low, it still diminishes our precision rate. We perform moderately well on test sets including medium-difficult anomalies; however, our system is unable to capture all such types during long periods due to a combination of over-labeling and relatively "normal"-appearing values in individual data streams.

The domain expert is very pleased with the performance of the model. Virtually all existing data QA tools only work by comparing multiple data streams. We are currently deploying the model at the H. J. Andrews LTER site. The raw data will be processed by the model and then immediately posted on the web site (along with a disclaimer that an experimental automated QA process is being used). This will significantly enhance the timeliness and availability of the data. The manual QA process will still be performed later, but using the model to focus the expert's time and attention.

To detect more subtle anomaly types (swapping between sensor leads, snow pack, etc.), our model must exploit the spatiotemporal correlations between sensors. Future research will investigate Gaussian Processes [27, 17] as a method for capturing the spatial correlation between multiple sensors across and within sites, such as the case in Kriging [18, 4]. In addition to providing a means of detecting additional sensor faults, this model extension will allow us to predict with greater certainty the actual temperature in situations where at least two of the four sensors are functioning correctly.

Bibliography

[1] H.B. Aradhye. Sensor fault detection, isolation, and accommodation using neural networks, fuzzy logick, and bayesian belief networks. Master's thesis, University of New Mexico, Albuquerque, NM, 1997.

[2] Stefan Arnborg. Efficient algorithms for combinatorial problems on graphs with bounded decomposability-a survey. *BIT*, 25(1):2–23, 1985.

[3] Chris Chatfield. *Time-Series Forecasting*. Chapman & Hall/CRC, New York, NY, 2000.

[4] Noel A.C. Cressie. *Statistics for Spatial Data*. Wiley-Interscience, Wiley, NY, 1993.

[5] Christopher Daly, K. Redmond, W. Gibson, M. Doggett, J. Smith, G. Taylor, P. Pasteris, and G. Johnson. Opportunities for improvements in the quality control of climate observations. In *15th AMS Conference on Applied Climatology*, Savannah, GA, June 2005. American Meteorological Society.

[6] Thomas Dean and Keiji Kanazawa. Probabilistic temporal reasoning. In *AAAI*, pages 524–529, 1988.

[7] Rina Dechter. Bucket elimination: A unifying framework for probabilistic inference. In E. Horvitz and F. Jensen, editors, *Twelthth Conf. on Uncertainty in Artificial Intelligence*, pages 211–219, Portland, Oregon, 1996.

[8] Rina Dechter. Inference in gaussian and hybrid bayesian networks. Course: *ICS-275B: Network-Based Reasoning - Bayesian Networks*, 2005. University of California, Irvine.

[9] David J. Hill and Barbara S. Minsker. Automated fault detection for in-situ environmental sensors. In *7th International Conference on Hydroinformatics*, Nice, France, 2006.

[10] David J. Hill, Barbara S. Minsker, and Eyal Amir. Real-time bayesian anomaly detection for environmental sensor data. In *Proceedings of the 32nd conference of IAHR*, Venice, Italy, 2007. International Association of Hydraulic Engineering and Research.

[11] Victoria Hodge and Jim Austin. A survey of outlier detection methodologies. *Artif. Intell. Rev.*, 22(2):85–126, 2004.

[12] P.H. Ibarguengoytia, L.E. Sucar, and S. Vadera. A probabilistic model for sensor validation. In E. Horvitz and F. Jensen, editors, *Twelthth Conf. on Uncertainty in Artificial Intelligence*, pages 332–333, Portland, Oregon, 1996.

[13] Rolf Isermann. Model-based fault detection and diagnosis: Status and applications. In *Annual Reviews in Control*, volume 29, pages 71–85. St. Petersburg, Russia, 2005.

[14] Frank Jensen, Finn Jensen, and Soren Dittmer. From influence diagrams to junction trees. In *Proceedings of the 10th Annual Conference on Uncertainty in Artificial Intelligence (UAI-94)*, pages 367–37, San Francisco, CA, 1994. Morgan Kaufmann.

[15] S.L. Lauritzen. Propogation of probabilities, means, and variance in mixed graphical association models. *Journal of The American Statistical Association*, 87(420):1098–1108, 1992.

[16] S.L. Lauritzen and N. Wermuth. Graphical models for associations between variables, some of which are qualitative and some quantitative. *The Annals of Statistics*, 17(1):31–57, 1989.

[17] David J.C. MacKay. *Information Theory, Inference, and Learning Algorithms.* Cambridge University Press, Cambridge, UK, 2003.

[18] G. Matheron. Principles of geostatistics. *Economic Geology*, 53(8):1246–1266, December 1963.

[19] W. McKee. Meteorological data from benchmark stations at the andrews experimental forest: Long-term ecological research. Corvallis, OR: Forest Science Data Bank: MS001, 2005.

[20] N. Mehranbod, M. Soroush, M. Piovos, and B. A. Ogunnaike. Probabilistic model for sensor fault detection and identification. *AIChe Journal*, 49(7):1787–1802, 2003.

[21] M. Mourad and J.L. Bertrand-Krajewski. A method for automatic validation of long time series of data in urban hydrology. *Water Science & Technology*, 45(4-5):263–270, 2002.

[22] Kevin P. Murphy. Inference and learning in hybrid bayesian networks. Technical Report UCB/CSD-98-990, University of California, Berkeley, California, January 1998.

[23] Kevin P. Murphy. A variational approximation for bayesian networks with discrete and continuous latent variables. In *UAI*, pages 457–466. Morgan Kaufmann, 1999.

[24] A. E. Nicholson and J. M. Brady. Sensor validation using dynamic belief networks. In *Proceedings of the eighth conference on Uncertainty in Artificial Intelligence*, pages 207–214, San Francisco, CA, USA, 1992. Morgan Kaufmann Publishers Inc.

[25] Judea Pearl. *Probabilistic Reasoning in Intelligent Systems: Networks of Plausible Inference*. Morgan Kaufmann Publishers Inc., San Francisco, CA, USA, 1988.

[26] Lawrence R. Rabiner. A tutorial on hidden markov models and selected applications in speech recognition. In *Readings in speech recognition*, pages 267–296. Morgan Kaufmann Publishers Inc., San Francisco, CA, USA, 1990.

[27] Carl Edward Rasmussen and Christopher K. I. Williams. *Gaussian Processes for Machine Learning*. The MIT Press, Cambridge, MA, 2006.

[28] Ben Y. Reis, Marcello Pagano, and Kenneth D. Mandl. Using temporal context to improve biosurveillance. *Proceedings of the National Academy of Science*, 100(4):1961–1965, 2003.

[29] Stuart Russell and Peter Norvig. *Artificial Intelligence: A Modern Approach*. Pearson Education, Inc., Upper Saddle river, New Jersey, 2003.

[30] A. Szalay and J. Gray. The world-wide telescope, an archetype for online science. Technical Report MSR-TR-2002-75, MSR, 2002.

[31] Ling Wang, Marco F. Ramoni, Kenneth D. Mandl, and Paola Sebastiani. Factors affecting automated syndromic surveillance. *Artificial Intelligence in Medicine*, 34(3):269–278, 2005.